Amino Acids (2012) 43:1761–1777
DOI 10.1007/s00726-012-1261-7

ORIGINAL ARTICLE

Antimicrobial lipopeptaibol trichogin GA IV: role of the three Aib residues on conformation and bioactivity

Marta De Zotti · Barbara Biondi · Yoonkyung Park · Kyung-Soo Hahm · Marco Crisma · Claudio Toniolo · Fernando Formaggio

Received: 13 February 2012 / Accepted: 28 February 2012 / Published online: 7 April 2012

Abstract The lipopeptaibol trichogin GA IV is a natural, non-ribosomally synthesized, antimicrobial peptide remarkably resistant to the action of hydrolytic enzymes. This feature may be connected to the multiple presence in its sequence of the non-coded residue α-aminoisobutyric acid (Aib), which is known to be responsible for the adoption of particularly stable helical structures already at the level of short peptides. To investigate the role of Aib residues on the 3D-structure and bioactivity of trichogin GA IV, we synthesized and fully characterized four analogs where one or two Aib residues are replaced by L-Leu. Our extensive conformational studies (including an X-ray diffraction analysis) and biological assays performed on these analogs showed that the Aib to L-Leu replacements do not affect the resistance to proteolysis, but modulate the bioactivity of trichogin GA IV in a 3D-structure related manner.

Keywords Antibiotics · Bioactivity · Conformational analysis · Membranes · Peptides · C^{α}-Tetrasubstituted α-amino acids

Abbreviations

Aib	α-Aminoisobutyric acid
AMPs	Antimicrobial peptides
CF	5(6)-Carboxyfluorescein
CFU	Colony forming unit
Ch	Cholesterol
DIEA	*N*,*N*′diisopropylethylamine
DMEM	Dulbecco's minimal Eagle medium
DMSO	Dimethylsulfoxide
DOPC	1,2-dioleyl-*sn*-*glycero*-3-phosphocholine
EDC	*N*-ethyl, *N*′-[3-(dimethylamino)propyl] carbodiimide
ESI	Electrospray ionization
Fmoc	Fluorenyl-9-methyloxycarbonyl
HaCaT	Human adult low-calcium high temperature
HATU	*O*-(7-azabenzotriazol-1-yl)-1,1,3,3 tetramethyluronium hexafluorophosphate
HBTU	*O*-(benzotriazol-1-yl)-1,1,3,3 tetramethyluronium hexafluorophosphate
HFIP	1,1,1,3,3,3-hexafluoroisopropanol
HMBC	Heteronuclear multiple bond coherence
HMQC	Heteronuclear multiple quantum coherence
HOAt	7-aza-1-hydroxy-benzotriazole
HOBt	1-hydroxy-benzotriazole
hRBCs	Human red blood cells
Lol	Leucinol
MeOH	Methanol
MES	2-(N-morpholino) ethanesulfonic acid
MIC	Minimal inhibitory concentration
MTT	3-(4,5-dimethylthiazol-2-yl)-2,5-diphenyl-2H-tetrazolium

Electronic supplementary material The online version of this article (doi:10.1007/s00726-012-1261-7) contains supplementary material, which is available to authorized users.

M. De Zotti (✉) · B. Biondi · M. Crisma · C. Toniolo · F. Formaggio
ICB, Padova Unit, CNR, Department of Chemistry, University of Padova, 35131 Padova, Italy
e-mail: marta.dezotti@unipd.it

Y. Park
Department of Biotechnology, Chosun University, 501-759 Gwangju, Korea

K.-S. Hahm
Department of Cellular Molecular Medicine, School of Medicine, Chosun University, 501-759 Gwangju, Korea

*n*Oct	*n*-Octanoyl
PBS	Phosphate buffered saline
RMSD	Root-mean-square deviation
SDS	Sodium dodecylsulphate
SPPS	Solid-phase peptide synthesis
SUVs	Small unilamellar vesicles
TFA	Trifluoroacetic acid
Z	Benzyloxycarbonyl

Introduction

In general, antimicrobial peptides (AMPs) act by altering the permeability of cell membranes (Tossi et al. 2000; Zasloff 2002; Brogden 2005; Papo and Shai 2005; Hancock and Sahl 2006). Thus, the absence of a well defined target limits the likelihood that bacteria develop resistance. Many AMPs were studied as lead compounds for novel antibacterial drugs, but few of them were approved for clinical use (Gordon et al. 2005; Zhang and Falla 2006; Marr et al. 2006). This failure is due mainly to two factors: (1) The general high toxicity of the natural antimicrobial peptides against eukaryotic cells (hemolysis, nephrotoxicity, neurotoxicity, and neuromuscular blockade). (2) Their rapid enzymatic degradation, especially in living systems. The AMPs hydrolytic stability is of crucial importance, because the molecules must survive in circulation for a relatively long time to exert an effective therapeutic action. In this connection, peptaibiotics (Toniolo and Brückner 2009), a group of natural AMPs, are particularly attractive. They are characterized by a high amount of non-coded α-amino acids, e.g. Aib (Brückner et al. 1991; Chugh and Wallace 2001; Toniolo et al. 2001a; Degenkolb et al. 2003). Their characteristic features are: (1) Significant resistance to the action of hydrolytic enzymes (Yamaguchi et al. 2003; De Zotti et al. 2009, 2011, 2012). (2) A very stable helical structure (even if the sequence is <10-residue long) (Toniolo and Brückner 2009). The widespread presence of Aib, a sterically demanding residue and a known helix inducer (Karle and Balaram 1990; Toniolo et al. 2001b), explains, at least in part, these properties.

Peptaibiotics are produced by fungi (to defend themselves from other microorganisms) by non-ribosomal synthesis in the form of heterogeneous mixtures, that often contain dozens of sequences (differing even for a single amino acid residue) (Toniolo and Brückner 2009). Therefore, it is difficult to isolate pure peptaibiotics in good amount from the natural sources. Since the chemical synthesis of peptaibiotics [especially through solid-phase peptide synthesis (SPPS)] is not a routine work (Formaggio et al. 2003; Hjørringgaard et al. 2009; Weigelt et al. 2012), for many years it remained a prerogative of a few specialized groups. These difficulties mainly stem from lack of reactivity of the sterically hindered, C^{α}-tetrasubstituted Aib residues, but also from the presence of the C-terminal 1,2-amino alcohol (resins preloaded with this moiety became commercially available only few years ago).

Trichogin GA IV (Toniolo et al. 1996a; Peggion et al. 2003) is a 10-mer member of a sub-class of peptaibiotics termed *lipopeptaibols* (Toniolo et al. 2001a), carrying a fatty acyl moiety at the N-terminus. Its primary structure is: *n*Oct-Aib^{1}-Gly-L-Leu-Aib-Gly^{5}-Gly-L-Leu-Aib-Gly-L-Ile^{10}-L-Lol. Trichogin GA IV and some of its analogs exhibit a strong activity against Gram-positive bacteria, in particular the methicillin-resistant *Staphylococcus aureus*, with low hemolysis and a remarkable resistance to proteolytic degradation (De Zotti et al. 2009). Here, we describe synthesis, conformational studies, and bioactivity of four analogs of trichogin GA IV with the aim at (1) identifying the amino acids essential for its activity, (2) increasing its antimicrobial properties without enhancing its hemolytic effect and (3) shedding light on the mechanism driving its resistance to enzymatic degradation.

To this end, in these analogs we replace one or two of the Aib residues with L-Leu. Among protein amino acids, Leu is one of the best helix-supporting residues, but still it is much less effective than Aib (Karle and Balaram 1990; Toniolo et al. 2001b). Also, the Aib lipophilicity is considerably enhanced in Leu.

Materials and methods

Synthesis

Fmoc-amino acids were supplied from Novabiochem (Merck Biosciences, La Jolla, CA, USA), and all other amino acid derivatives and reagents for peptide synthesis were purchased from Sigma-Aldrich (St. Louis, MO, USA). EDC, HATU and HOAt were purchased from GLS (Shanghai, China). Assembly of peptides on the Advanced ChemTech (Louisville, KY, USA) 348 Ω peptide synthesizer was performed on a 0.05 mmol scale by the FastMoc methodology [HBTU, HOBt, DIEA, single acylation protocol, 45 min coupling time, *N*-methylpyrrolidin-2-one as the solvent], starting with L-Lol 2-chlorotrityl resin (Iris Biotech, Marktredwitz, Germany) (110 mg, loading 0.45 mmol g^{-1}). The deprotection of the Fmoc group was performed with a 20 % piperidine solution in *N*,*N*-dimethylformamide. The coupling steps involving Aib residues, carried out in presence of HATU, were doubled and followed by a capping protocol using acetic anhydride in a large excess. The *n*Oct moiety at the N-terminus was introduced using the preformed activated ester of

n-octanoic acid, obtained by reaction with an equivalent amount of EDC and HOAt, in the presence of *N*-methylmorpholine. The 1 hr coupling procedure was repeated twice. Cleavage of peptides from the resin was achieved by treatment with 30 % HFIP in dichloromethane. The filtrate was collected and the step repeated three times (the last one was performed overnight). Then, the solution was concentrated under a flow of N_2. The crude peptides were purified by flash chromatography and characterized by analytical RP-HPLC on a Vydac C_4 column (4.6 × 250 mm, particle size: 5 μ, pore size: 300 Å) using a Dionex (Sunnyvale, CA, USA) P680 HPLC pump with an automated sample injector ASI-100 and spectrophotometric detection (flow rate 1.0 ml/min; λ: 226 nm; room temperature) with a binary elution system: A, 0.1 % TFA in H_2O; B, 0.1 % TFA in CH_3CN/H_2O (9/1 *v*/*v*); gradient 50–90 % B in 30 min. ESI–MS was performed by using a PerSeptive Biosystem Mariner instrument (Framingham, MA, USA).

Circular dichroism spectroscopy

The CD spectra were measured on a Jasco (Hachioji City, Japan) model J-715 spectropolarimeter equipped with a Haake thermostat (Thermo Fisher Scientific, Waltham, MA, USA). Baselines were corrected by subtracting the solvent contribution. Fused quartz cells of 0.5, 0.2, and 0.1 mm path length (Hellma, Mühlheim, Germany) were used. The values are expressed in terms of $[\theta]_T$, the total molar ellipticity (deg × cm^2 × $dmol^{-1}$). Spectrograde MeOH 99.9 % (Acros Organic, Geel, Belgium) was used as solvent.

IR absorption spectroscopy

The FT-IR absorption spectra were recorded at 293 K using a Perkin-Elmer model 1720X FT-IR spectrophotometer, nitrogen flushed, equipped with a sample-shuttle device, at 2 cm^{-1} nominal resolution, averaging 100 scans. Solvent (baseline) spectra were recorded under the same conditions. For spectral elaboration, the software SPECTRACALC, provided by Galactic (Salem, MA, USA), was employed. Cells with path lengths of 1.0 and 10 mm (with CaF_2 windows) were used. Spectrograde deuterated chloroform (99.8 %, d_2) was purchased from Merck (Darmstadt, Germany).

X-ray diffraction

Crystals, in the shape of thin plates, were grown by slow evaporation from a MeOH solution. A specimen of about 0.22 × 0.18 × 0.01 mm^3 was glued on the tip of a glass fiber. X-ray diffraction data were collected at room temperature with an Agilent Technologies Gemini E four-circle kappa diffractometer equipped with a 92 mm EOS CCD detector, using graphite monochromated Cu Kα radiation (λ = 1.54178 Å). The sample to detector distance was 50 mm. A total of 1,911 frames were collected by 1.0° ω oscillation with exposure times of 20 or 60 s, depending on the θ values, in the 2.44–44.99° θ range. The crystal did not significantly diffract beyond 1.1 Å resolution. Data collection and reduction were performed with the CrysAlisPro software (version 1.171.34.49, Agilent Technologies). A semi-empirical absorption correction based on the multi-scan technique using spherical harmonics, implemented in the SCALE3 ABSPACK scaling algorithm, was applied. Crystals are triclinic, space group P1, with cell parameters a = 9.6979(6) Å, b = 10.2472(7) Å, c = 36.701(2) Å, α = 87.186(5)°, β = 85.108(5)°, γ = 61.811°(6). Cell volume and density considerations pointed to the likely occurrence of two peptide molecules/asymmetric unit. Cell transformation in search for higher symmetry suggested a pseudomonoclinic C cell with a = 9.698 Å, b = 18.064 Å, c = 36.701 Å, α = 89.43°, β = 94.89°, γ = 89.95°, and Z = 4 (one independent peptide molecule). However, such a possibility was ruled out, since data reduction assuming the monoclinic C cell would lead to a value for R_{int} as high as 0.417. The structure was solved ab initio by seeding the dual-space direct methods of the SHELXD program (Sheldrick 2008) by a 6D search (through random rotation and translation) for a rigid fragment consisting of the backbone and some C^{β} atoms of the L-enantiomer of one of the two independent, helical molecules present in the X-ray diffraction structure of racemic trichogin GA IV (Toniolo et al. 1994). The solution allowed the location of 140 atoms in two, nearly complete, peptide molecules as well as two co-crystallized water molecules. The positions of the remaining atoms were recovered from subsequent difference Fourier maps interleaved by cycles of refinement. Residues are numbered 1 to 11 in molecule **A** and 21 to 31 in molecule **B**. In both peptide molecules the hydroxyl group of the C-terminal L-Lol is disordered over two positions (atoms O11 and O′11 in molecule **A**, while O31 and O′31 in molecule **B**), to which half-occupancy was imposed. Refinement was carried out by full-matrix least-squares procedures on F^2, using all data, by application of the SHELXL 97 program (Sheldrick 2008). Some cycles of isotropic refinement of all non-H atoms, with restraints on some of the bond distances and angles, led to R_1 = 0.130. A fully unrestrained anisotropic refinement could not be performed, owing to the limited resolution of the dataset which, in turn, determines a poor data/parameters ratio. Therefore, the anisotropic refinement of all non-H atoms was carried out in combination with the imposition of similarity restraints on the anisotropic displacement

parameters of atoms bonded to each other ("SIMU" command in SHELXL 97) (Sheldrick 2008). H-atoms of the peptide molecules were calculated at idealized positions and refined using a riding model. The positions of the H-atoms bonded to the two co-crystallized water molecules were inferred from a likely H-bonding scheme and they were not refined. Overall, many crystallographic parameters suffer from the far from optimal crystal size and quality. In particular, large displacement parameters ($U_{eq} \geq 0.20$ Å^3) characterize the two co-crystallized water molecules, as well as the atoms belonging to the *n*Oct chain and some side chains. This latter observation may suggest the possible occurrence of disorder. However, the data did not support a suitable model to unravel the putative disorder satisfactorily. In any case, it is our contention that the basic conformational features of the molecules, as discussed in this work, are unambiguously established. Formula: $C_{54}H_{99}N_{11}O_{12} \times H_2O$; formula weight: 1112.46; triclinic, space group P1; unit cell parameters: $a = 9.6979(6)$ Å, $b = 10.2472(7)$ Å, $c = 36.701(2)$ Å, $\alpha = 87.186(5)°$, $\beta = 85.108(5)°$, $\gamma = 61.811°(6)$; $V = 3202.8(3)$ Å^3; $Z = 2$; $D_{calcd} = 1.154$ Mg m^{-3}; crystal size: $0.22 \times 0.18 \times 0.01$ mm^3; $2\theta_{max} = 89.98°$; reflections collected: 20,472; independent reflections: 9,978 [$R_{int} = 0.068$]; $\mu = 0.673$ mm^{-1}; max/min transmission: 1.0000/0.8018; data/restraints/parameters 9978/1139/1424; $R_1 = 0.089$ [on $F \geq 4\sigma(F)$]; $wR_2 = 0.250$ (on F^2, all data); goodness of fit on F^2: 1.053; largest peak and hole in the final difference Fourier map: 0.586 and −0.292 e Å^{-3}. CCDC 852943 contains the supplementary crystallographic data for this paper. These data can be obtained from the Cambridge Crystallographic Data Centre via http://www.ccdc.cam.ac.uk/data_request/cif.

Nuclear magnetic resonance spectrometry

Samples for NMR spectrometry were dissolved in water (9:1 H_2O/D_2O) containing (100 mM) SDS-d_{25} or in MeOH-d_3 solution (peptide concentrations: about 2 and 1 mM, respectively). The pH of the SDS-containing solution was adjusted at 5.53 by adding 5 µl of a 6 M HCl solution. The spectra were recorded at 313 K. All NMR experiments were performed on a Bruker Avance DMX-600 spectrometer using the TOPSPIN 1.3 software package. Presaturation of the H_2O solvent signal was obtained using a WATERGATE gradient program. All homonuclear spectra were acquired by collecting 512 experiments, each one consisting of 64–80 scans and 2 K data points. The spin systems of the protein amino acid residues were identified using standard DQF-COSY (Rance et al. 1983) and CLEAN-TOCSY (Bax and Davis 1985; Griesinger et al. 1988) spectra. In the latter case, the spin-lock pulse sequence was 70 ms long. The assignment of the two methyl groups belonging to the same Aib residue was obtained by means of ^{1}H–^{13}C 2D correlation spectra. To optimize the digital resolution in the carbon dimension, HMQC (Bax and Subramanian 1986) and HMBC (Bax and Summers 1986) experiments were acquired using selective excitation by means of Gaussian-shaped pulses with 1 % truncation (Bauer et al. 1984; Emsley and Bodenhausen 1989).

The C^{β}-selective HMQC experiments with gradient coherence selection (Bax et al. 1983) were recorded with 320 t_1 increments, of 300 scans and 2 K points each (Bax and Subramanian 1986). A spectral width of 16 ppm centered at 22 ppm in F1 was used, yielding a digital resolution of 2.36 Hz/pt prior to zero filling. HMBC experiments with selective excitation in the CO region were performed using a long-range coupling constant of 7.5 Hz, a spectral width in F1 of 15 ppm centered at 176 ppm, 250 t_1 experiments of 640 scans, and 4 K points in F2. The digital resolution in F1, prior to zero filling, was 2.2 Hz/pt. NOESY experiments were used for sequence specific assignment. To avoid the problem of spin diffusion, the build-up curve of the volumes of the NOE cross-peaks as a function of the mixing time (50 to 500 ms) was determined first (data not shown). The mixing time of the NOESY experiment used for interproton distance determination was 150 ms, that is, in the linear part of the NOE build-up curve. Interproton distances were obtained by integration of the NOESY spectrum using the SPARKY 3.111 software package. The calibration was based on the average of the integration values of the cross-peaks due to the interactions between the two Aib β-geminal protons set to a distance of 1.78 Å. Distance geometry and MD calculations were carried out using the random simulated annealing (rSA) protocol of the XPLOR-NIH 2.9.6 program (Schwieters et al. 2003). For distances involving equivalent or non-stereo-assigned protons, an r^{-6} averaging was used. The MD calculations involved a minimization stage of 100 cycles, followed by SA and refinement stages. The SA consisted of 30 ps of dynamics at 1,500 K (10,000 cycles in 3 fs steps) and of 30 ps of cooling from 1,500 to 100 K in 50 K decrements (15,000 cycles in 2 fs steps). The SA procedure, in which the weights of NOE and non-bonded terms were gradually increased, was followed by 200 cycles of energy minimization. In the SA refinement stage, the system was cooled from 1,000 to 100 K in 50 K decrements (20,000 cycles, in 1 fs step). Finally, the calculations were completed with 200 cycles of energy minimization using a NOE force constant of 50 kcal/mol. The generated structures were visualized using the MOLMOL (Korady et al. 1996) (version 2K.2) program.

Antibacterial activity

In the antibacterial activity assay, the broth microdilution method was used. Bacteria were grown to the

mid-logarithmic phase in a medium at 37 °C. The cells were collected and suspended with PBS. Twofold serial dilutions of each peptide, from 1 to 64 μM, in PBS were arranged in sterile 96-well plates. Then, an aliquot of cell suspension was added to each well. The cell count was 2×10^5 CFU/ml. After incubation for 12 h at 37 °C, the inhibition of bacterial growth was assessed by measuring the absorbance at 620 nm with a Microplate ELISA reader.

Antifungal activity

To determine the MIC values for the peptides against various fungal pathogens, fungi were grown in YPD media at 28 °C. The antibacterial activity of each peptide was tested using the microdilution assay. Serial dilutions of peptides were performed in PBS in sterile 96-well plate. Aliquots of a bacterial suspension were added at 2×10^4 CFU/ml in PBS. The plates were incubated for 24 h at 28 °C. At the end of the incubation, growth or germination of fungi was evaluated microscopically, using an inverted microscope, and turbidity of each well was also measured following the absorbance at 595 nm by use of a microtiter reader.

Hemolytic activity

The hemolytic activity of the peptides was determined using hRBCs from healthy donors that were collected on heparin. Fresh hRBCs were washed three times in PBS by centrifugation for 10 min at 800*g* and resuspension in PBS. The peptides were dissolved in the minimum amount of DMSO, diluted with PBS to the desired concentration (in the range 10–500 μg/ml) and then added to 100 μl of stock hRBCs suspended in PBS (final hRBCs concentration: 8 %, *v*/*v*). The maximum amount of DMSO in each solution was 1.4 %. The samples were incubated with agitation for 1 h at 37 °C and centrifuged at 800*g* for 10 min. The absorbance of the supernatant was measured at 414 nm. Controls for zero hemolysis (blank) and 100 % hemolysis consisted of hRBCs suspended in PBS and 1 % Triton X-100, respectively. The percentage of hemolysis was calculated using the following equation: % hemolysis = $[(A_{414\ nm}$ with peptide solution $- A_{414\ nm}$ in PBS)/$(A_{414\ nm}$ with 0.1 % Triton X-100 $- A_{414\ nm}$ in PBS)] $\times$ 100. Each measurement was made in triplicate.

Cytotoxicity

HaCaT keratinocyte cells were cultivated in DMEM at 37 °C and 5 % CO_2 for 5–7 days. Assays were performed by incubation of 2 × 103 cells with various concentrations of peptides for 19 h at 37 °C and 5 % CO_2 in a 96-well plate. Triton X-100 (0.1 % final concentration) was used as a negative control and the pure medium assay was used as a positive control. Proliferation and viability were determined by MTT bromide assay. The plate was then incubated for 24 h before adding 50 μl of MTT solution to each well. The medium containing MTT was removed and 100 μl of DMSO were added. Cells were incubated for 10 min at 37 °C with gentle shaking. The optical density was read at 550 nm using an enzyme-linked immunosorbent assay plate reader after 2 h of incubation. Cell viability was determined relative to the control. All assays were performed in triplicate.

Enzymatic stability assay

Peptides were dissolved in an enzyme buffer (for trypsin, chymotrypsin and endoproteinase Glu-C: 50 mM Tris–HCl, pH 7.8; for pepsin: 20 mM sodium acetate, pH 4.6; for papain: 5 mM MES, pH 6.2; for elastase: 0.1 M Tris–HCl, pH 8.3, 0.01 % sodium azide; for pronase E: 0.02 M Tris–HCl, pH 7.6; for subtilisin A: 20 mM Tris–HCl, 2 mM $CaCl_2$, pH 8.0). The enzyme/peptide ratio (*w*/*w*) was 1/250. Peptide/enzyme mixtures were incubated at 37 °C overnight. Samples were analyzed using C_{18} RP-column on an HPLC system. Appropriate gradients from 40 to 95 % B solution for 20 min were applied, using as eluant solutions: A(H_2O/0.1 % TFA) and B(CH_3CN/0.1 % TFA). Absorption was monitored at 215 nm.

Plasma stability assay

Ten microlitre of a solution of each peptide (1 mg/ml) were dissolved in 90 μl of plasma and incubated at 37 °C for 2 h. Subsequently, 20 μl of trichloroacetic acid (15 % *v*/*v* in water) were added and samples were incubated at 4 °C for 20 min. The samples were then centrifuged at 13,000 rpm for 10 min. After centrifugation, supernatants were analyzed using C_{18} reverse-phase column on an HPLC system. Appropriate programmed gradients from 40 to 95 % B for 20 min were applied using eluents A: H_2O/0.05 % TFA and B: CH_3CN/0.05 % TFA. Absorption was monitored at 215 nm.

Results and discussion

Peptide synthesis

We prepared a set of four novel trichogin GA IV analogs, the primary structure of which is given below, where the three Aib residues at positions 1, 4, and 8 are replaced by one or two L-Leu residues.

*n*Oct- L-**Leu**^{1}-Gly- L-Leu-Aib-Gly^5-Gly- L-Leu-Aib-Gly-L-Ile^{10}- L-Lol (**L1**)

*n*Oct-Aib[1]-Gly- L-Leu- L-**Leu**-Gly[5]-Gly- L-Leu-Aib-Gly- L-Ile[10]- L-Lol (**L4**)
*n*Oct-Aib[1]-Gly- L-Leu-Aib-Gly[5]-Gly- L-Leu- L-**Leu**-Gly- L-Ile[10]- L-Lol (**L8**)
*n*Oct- L-**Leu**[1]-Gly- L-Leu-Aib-Gly[5]-Gly- L-Leu- L-**Leu**-Gly- L-Ile[10]- L-Lol (**L1,8**)

For the automatic SPPS of the above-mentioned trichogin GA IV analogs we applied our improved protocol for the preparation of peptaibols (De Zotti et al. 2011, 2012) illustrated in Fig. 1. Each of these four syntheses, performed in parallel on the L-Lol substituted 2-chlorotrityl resin (Barlos et al. 1991; Bollhagen et al. 1994; Kocsis et al. 2006) as described in detail in the "Materials and methods" section, required 30 h (Table 1). Basically, our procedure involves: (1) Use of the strong activating method via HATU or EDC/HOAt in the coupling reactions with Aib residues, and (2) Cleavage from the 2-chlorotrityl resin (Kocsis et al. 2006) in three cycles of 30 % HFIP in distilled CH_2Cl_2 (the last cycle performed overnight). The desired final peptides were isolated in 75–80 % average yield with a purity of about 98 %, as highlighted by analytical RP-HPLC of the crude products (Fig. 2; Table 1).

The peptides were additionally characterized by ESI–MS (Table 1) and NMR spectrometry. The recently reported SPPS of trichogin GA IV, performed according to a different procedure, resulted in a 20 % isolated yield (Hjørringgaard et al. 2009).

Circular dichroism and infrared absorption analyses

A preliminary analysis of the solution preferred conformations of the **L1**, **L4**, **L8**, and **L1,8** trichogin GA IV analogs synthesized in this work, as compared to that of the natural prototypical compound, were performed using CD and FT-IR absorption spectroscopies in different solvents. Previous studies (Toniolo et al. 1996a; Peggion et al. 2003) highlighted the intriguing ability of trichogin GA IV to interact with lipid membranes. For this reason, our analysis included two membrane-mimetic environments: micelles of SDS investigated by CD and the solvent $CDCl_3$, the polarity of which resembles that of the core of a lipid membrane (used in the FT-IR absorption measurements).

Far-UV CD spectra were acquired in the polar solvent MeOH and in a 100 mM SDS aqueous solution. The occurrence in each spectrum of two negative maxima near 205 and 222 nm of moderate intensities and one positive maximum at about 195 nm (Beychock 1967; Manning and Woody 1991) (Fig. 3), indicates the presence of a right-handed, largely mixed α-/3_{10}-helical conformation (Toniolo and Benedetti 1991; Benedetti et al. 1992) for all peptides. By means of CD, we could extract an initial estimate of the prevailing helical type adopted in solution from the values of the ellipticity ratio $R = [\Theta]_{222}/[\Theta]_{205}$, known to be <0.35 for a high population of 3_{10}-helix and >0.70 for a high population of α-helix (Manning and Woody 1991; Toniolo et al. 1996b; Formaggio et al. 2000) (Table S1, Supporting Information).

For all compounds the R value was <0.3 in MeOH solution and around 0.6 in SDS. This observation is in agreement with the known tendency of trichogin GA IV to adopt a 3_{10}-helical conformation to a large extent in MeOH (Toniolo et al. 1996a; Monaco et al. 1998) and a well developed α-helical conformation in SDS. In conclusion, the four analogs exhibit an overall α-/3_{10}-helix ratio quite close to that shown by trichogin GA IV under the same experimental conditions, despite the reduction in the number of the helix-inducing Aib residues in their sequences (Monaco et al. 1998).

The conformations adopted by the four trichogin GA IV analogs were subsequently assessed by FT-IR absorption in $CDCl_3$. In Fig. S1 (Supporting Information) the spectra in the conformationally informative N–H stretching region are reported. The Aib to L-Leu substitutions did not affect the solubility in $CDCl_3$. The presence of a very strong band associated with H-bonded N–H groups near 3330 cm^{-1} (Bellamy 1966; Cung et al. 1972; Pysh and Toniolo 1977; Moretto et al. 1989) is indicative of the overwhelming

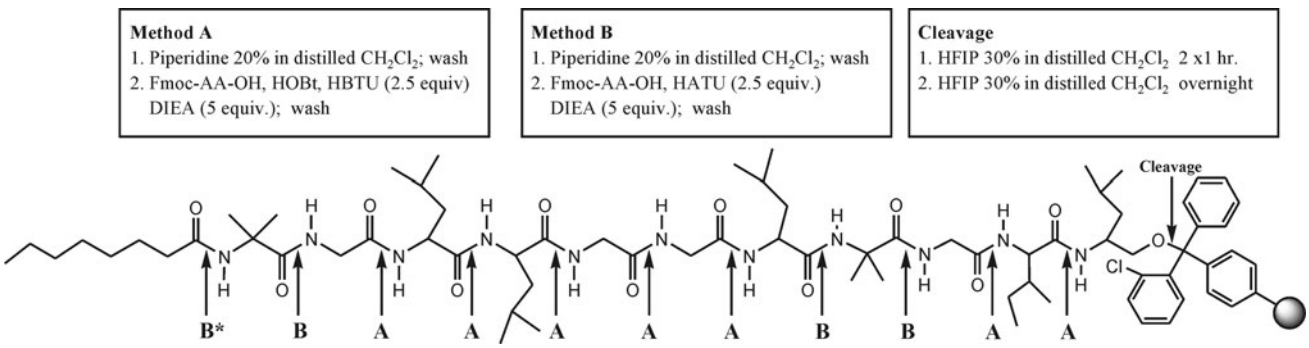

Fig. 1 Synthesis protocol for the preparation of the trichogin GA IV analogs (exemplified for **L4**). *B** coupling of the *n*Oct was performed using the activating method EDC/HOAt (2.5 equiv.)

Table 1 SPPS details and characterization data for the **L1**, **L4**, **L8**, and **L1,8** trichogin GA IV analogs

Peptide	Synthesis time (h)	Crude purity (%)	Yield (%)	MW_{calcd}	MW^{a}_{exp}	t_R (min)[b, c]
L1	30	98	80	1094.75	1094.74	15.4
L4	30	97	78	1094.75	1094.72	18.1
L8	30	98	75	1094.75	1094.73	16.3
L1,8	30	97	80	1121.78	1121.79	16.9

All syntheses were performed on a ACT348Ω peptide synthesizer and a 0.05 mmol scale using a preloaded L-Lol-chlorotrityl resin

[a] Data obtained by ESI–MS

[b] For the elution conditions, see "Materials and methods" section

[c] The corresponding t_R value for trichogin GA IV is 13.5 min

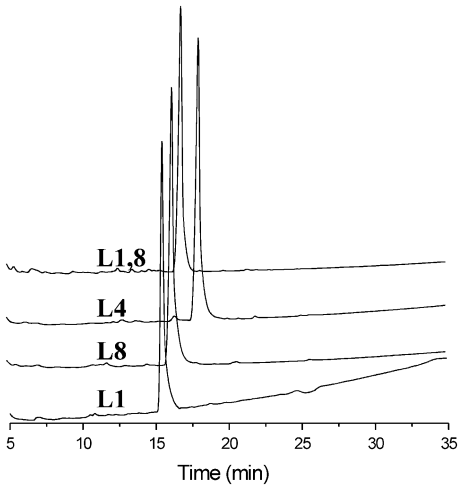

Fig. 2 Analytical RP-HPLC profiles obtained for the crude **L1**, **L4**, **L8**, and **L1,8** trichogin GA IV analogs

occurrence of a highly folded conformation stabilized by H-bonds in all peptides. The variation of peptide concentration (from 1 to 0.1 mM) alters only slightly the overall shape of the spectra (not shown). In summary, our preliminary CD and FT-IR absorption analysis indicates that the Aib to L-Leu replacements affect minimally the extent and type of the native helical conformation.

Biological activity

The antimicrobial activity of the four Aib-to-L-Leu trichogin GA IV analogs was investigated against two strains of Gram-positive bacteria (*Staphylococcus aureus* and *Staphylococcus epidermidis*), two strains of Gram-negative bacteria (*Escherichia coli* and *Pseudomonas aeruginosa*), and two types of fungi (*Candida albicans* and *Trichosporon beigelli*) (Table 2). As expected, no antifungal activity was detected for these compounds: indeed, trichogin GA IV is a fungal peptide.

All the investigated Aib-to-L-Leu substitutions removed the activity of trichogin GA IV against *E. coli*, thus indicating a relevant role played by the Aib residues present in the native sequence against this Gram-negative strain. The results obtained highlighted an enhanced activity against *S. aureus* for the **L1** and **L8** analogs with a MIC of 2 and 4 μg/ml, respectively, thus reaching and even ameliorating the antibacterial activity of the reference compound melittin (4 μg/ml) under the same conditions. Surprisingly, **L4** proved to be inactive even at a concentration higher than 64 μg/ml.

To further investigate the antibacterial properties of these compounds, we assessed their activity against *S. aureus* in 25 % plasma. The MIC values reported in Table 2 show that the inhibition of bacterial growth caused by the active peptides was still detectable even after 12 h of incubation. Moreover, the study of the stability of these peptides in plasma (Fig. S2, Supporting Information) underscores a significant long half-life time (about 1 h) for all the peptides examined.

The hemolytic activity of the four trichogin GA IV analogs was tested in comparison with that of the native peptaibol. We found that all analogs are not toxic for human erythrocytes even at very high concentrations (128 μg/ml; Fig. S3**A**, Supporting Information). Furthermore, the cytotoxicity assays conducted on HaCaT keratinocyte cells highlighted a reduced toxicity for all analogs with respect to trichogin GA IV (Fig. S3**B**, Supporting Information).

In summary, the substitution of one or two Aib residues by L-Leu allowed us to verify the relevance of the C^{α}-tetrasubstituted residues for the biological properties of trichogin GA IV. In particular: (1) When the replacement occurs at position 4 the antibiotic activity is completely lost, while when it occurs at position 1 or 8 the antibiotic activity is four- or two-times higher than that of the native compound. (2) All peptides investigated exhibit a very promising stability in plasma. (3) The enhanced hydrophobicities of the trichogin GA IV analogs with respect to that of the native compound are probably responsible for the absence of any hemolytic activity. (4) The cytotoxic activities against the HaCaT keratinocyte cells are significantly lower

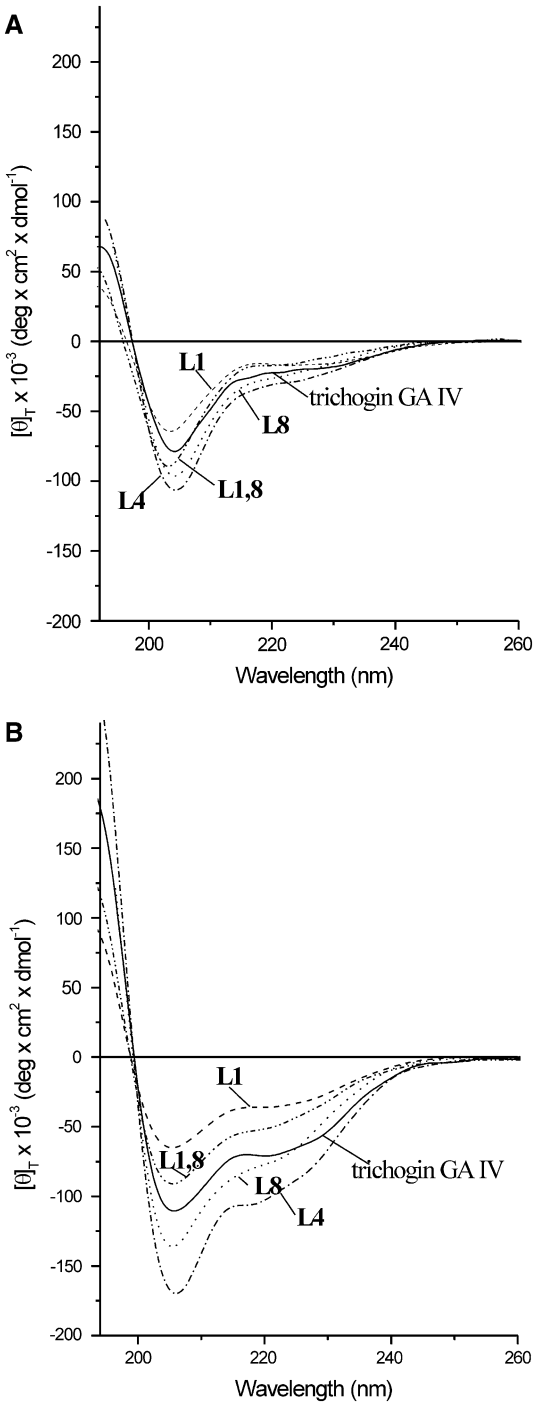

Fig. 3 Far-UV CD spectra of trichogin GA IV and its **L1**, **L4**, **L8**, and **L1,8** analogs in MeOH solution (**A**) (peptide concentration: 1 mM) and 100 mM SDS aqueous solution (**B**) (peptide concentration 1 mM)

than that of trichogin GA IV. Therefore, Aib[4] seems to be a key residue for the biological properties of trichogin GA IV. Among these analogs stable in plasma, **L1** and **L8** show the most remarkable activity against *S. aureus* (even higher than that of melittin for **L1**), no hemolytic activity, and a significantly low cytotoxicity.

Membrane activity

The membrane permeability properties of the synthetic analogs were tested in comparison with that of the native lipopeptaibol trichogin GA IV by measuring the induced leakage of CF entrapped in SUVs. For this investigation, the overall neutral, zwitter-ionic DOPC/Ch model membrane was exploited. The permeability effect of these trichogin GA IV analogs is quite remarkable and close to that of the native compound (Fig. S4, Supporting Information). It is known that the ability to induce permeability in a neutral membrane is often related to the hydrophobicity of the peptide investigated. This is probably the reason why **L1,8** exhibits the highest membrane activity. Conversely, **L1**, **L4**, and **L8** possess similar hydrophobicities. Therefore, the difference between their membrane permeability properties is expected to be related directly to their peculiar membrane affinities. The trends observed for these latter analogs nicely mirror their antibiotic activities, with **L4** being the least effective in inducing CF leakage. The histogram reported in Fig. 4A shows that, at the MIC of **L1** against *S. aureus* (2 μg/mL), the **L1**-induced membrane permeabilization (CF leakage from SUV) is approximately twofold that of **L4**. Even at the MIC of trichogin GA IV (8 μg/mL), **L4** is clearly less active (Fig. 4B). These results underscore the important role played by peptide–membrane interactions on the antimicrobial mechanism of the trichogin GA IV analogs. Indeed, the ability of these compounds to interact with the membrane bilayer is likely to be the main responsible for their biological activity. This aspecific mechanism, reducing the resistance-induction risks, makes them promising candidates as new antimicrobial agents.

Proteolytic stability

The intriguing stabilities of trichogin GA IV and its analogs in plasma (Fig. S2, Supporting Information) prompted us to assess their resistance to the action of several proteolytic enzymes. All of the compounds examined, even **L1,8** which contains only one Aib residue, proved to be resistant towards the proteolytic attack of elastase, pronase E, subtilisin A, pepsin, and papain for more than 4 h (data not shown). We conclude that the mechanism driving trichogin GA IV resistance to enzymatic degradation does not rely merely on the presence of Aib residues, but rather in a more complex series of concurrent factors.

Mechanism of bioactivity and 3D-structure–activity relationship

We already mentioned that trichogin GA IV is believed to act against bacteria with a membrane-interacting

Table 2 Antibacterial activity (MIC, μg/ml) for the **L1**, **L4**, **L8**, and **L1,8** trichogin GA IV analogs

Peptide	*S. aureus*		*S. epidermidis*	*E. coli*	*P. aeruginosa*
	PBS	25 % plasma[a]	PBS	PBS	PBS
Trichogin GA IV	8–16	32	>64	32	>64
L1	2	16	>64	>64	>64
L4	>64	>64	>64	>64	>64
L8	4	16	>64	>64	>64
L1,8	16–32	64	>64	>64	>64
Melittin	4	Not determined	2	2	4

[a] After 12 h incubation

mechanism. Even though the exact pathway of this phenomenon is not clear thus far, our published results point to the formation of peptide helical aggregates which permeate the bacterial membrane by forming pores (Mazzuca et al. 2005; Smeazzetto et al. 2011). In any case, it is clear that the secondary structure plays a crucial role in the bioactivity of trichogin GA IV. The intriguing biological behavior of peptide **L4** prompted us to investigate more deeply the 3D-structure adopted by this analog. On the basis of the results of the CD and FT-IR absorption spectroscopies discussed above, we did not observe any significant difference in the conformational properties of **L4** as compared to those of the other analogs. Therefore, we decided to exploit different physico-chemical techniques (2D-NMR and X-ray diffraction) capable to offer a more detailed picture of the conformation of this trichogin GA IV analog at the local level. For comparison, we decided to investigate also peptide **L1**, which shows the highest antibiotic activity.

Nuclear magnetic resonance analysis

The 2D-NMR spectra of **L1** and **L4** were recorded in an environment mimetic of negatively charged membranes, namely a (100 mM) SDS aqueous mixture. The proton resonances were fully assigned following the Wüthrich procedure (Wüthrich 1986). Moreover, to complete the assignments of the resonances of the Aib residues, the hetero-correlated ^{13}C–^{1}H C=O selective HMBC (Bauer et al. 1984; Bax and Summers 1986; Emsley and Bodenhausen 1989) and C^{β} selective HMQC (Bax et al. 1983; Bax and Subramanian 1986) 2D-NMR spectra were analyzed. For the configurational assignment of the two prochiral Aib methyl groups we used a selective HMQC experiment centered in the $^{\beta}CH_3$ region of the ^{13}C spectrum (20–40 ppm region). In the NOESY spectra of **L1** and **L4** in SDS aqueous solution, all $NH_i \rightarrow NH_{i+1}$ sequential cross-peaks are seen (Fig. S5, Supporting Information), which is a clear indication of the presence of a helical structure, thus confirming the above discussed findings. However, in **L4** the amide proton resonances are much more overlapped than in **L1**. This finding is often associated with some flexibility of the three-dimensional structure. In the fingerprint region of the NOESY spectrum of **L1** (Fig. 5), the 3_{10}-helical $C^{\alpha}H_i \rightarrow NH_{i+2}$ cross-peaks concomitantly occur with an α-helical $C^{\alpha}H_i \rightarrow NH_{i+4}$ cross peak, which points out the presence of a mixed 3_{10}-/α-helix conformation.

The NOESY fingerprint region for **L4** (Fig. 5) reveals a predominant 3_{10}-helical conformation. Surprisingly, no α-helical $C^{\alpha}H_i \rightarrow NH_{i+4}$ cross-peaks could be observed (in part because of the extensive overlapping of the signals in this spectrum). As it can be seen in Figs. 5 and S5 (Supporting Information), the NOESY spectrum of **L4** is characterized by an extensive overlapping of the amide proton resonances, which could not be resolved by changing the experimental conditions (temperature and/or peptide concentration). This observation prevented us from performing restrained molecular dynamics (MD) calculations on **L4**. In any case, the clear differences in the patterns of the medium-range connectivities found in the NOESY spectra of **L1** and **L4** suggest the presence of divergent overall structures for the two analogs. Under the same experimental conditions, **L4** presents fewer interresidue cross-peaks and no evidence for an α-helix, while **L1** exhibits a remarkable set of connectivities. This observation might imply a limited rigidity of the **L4** helical structure, which could be related to the occurrence of a conformational interchange at the level of the flexible -Gly^5-Gly^6- dipeptide segment promoted by the lack of the Aib residue in its proximity.

The better resolved cross-peaks found in the NOESY spectrum of **L1** allowed us to perform a more detailed conformational study by means of restrained MD calculations. After analysis of the build-up curve (not shown), the NOESY spectrum of **L1** with mixing time of 200 ms was chosen as the most suitable one. A summary of the significant interresidue cross-peaks found in this spectrum, given in Fig. 6, strongly indicates the presence of a 3_{10}-helical conformation throughout the sequence, with a short α-helical stretch in its N-terminal part. A total of 91

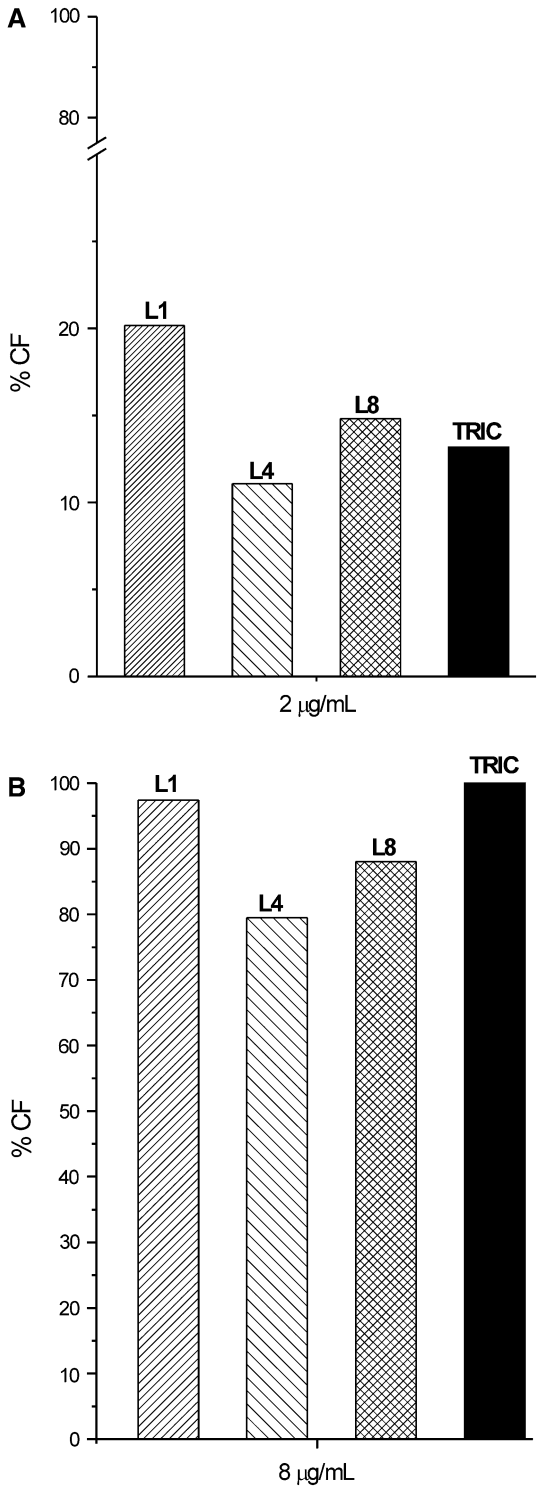

Fig. 4 Histograms of the induced CF leakage from SUVs (POPC/Ch 7:3) for trichogin GA IV and its three mono-substituted analogs at the MIC value of **L1** (**A**) and of trichogin GA IV (**B**) (lipid concentration 0.06 mM)

interproton distance restraints was derived (Table 3) and used in the random simulated annealing protocol. Out of the 150 3D-structures generated, 110 had violations to the NOE restraints lower than 0.5 Å. All structures converge to a straight helical conformation, with a backbone average RMSD of 0.18 (± 0.10) Å. The 58 structures with a total energy <268 kcal/mol were selected [backbone average RMSD 0.12 (± 0.05) Å]. Their representation is shown in Fig. 7.

The analysis of their averaged torsion angles (Table 4), confirms the coexistence of the α- and the 3_{10}-helical conformations. The lowest-energy 3D-structure is shown in Fig. 8, which highlights the amphiphilicity of the helix (one face is formed by the four Gly residues). In conclusion, the results of our MD calculations suggest the presence of a straight, mixed 3_{10}-/α-helical conformation throughout the sequence of the **L1** analog. The amphiphilicity of the **L1** helical structure in the membrane-mimetic environment investigated might be responsible for its high antibacterial activity.

Crystal-state conformational analysis

Among the four trichogin GA IV analogs, we succeeded in the crystallization of **L4**. The X-ray diffraction structure of **L4** is illustrated in Fig. 9. The asymmetric unit is composed of two independent peptide molecules (**A** and **B**) and two co-crystallized water molecules (Supporting Information). Amino acid residues are numbered 1 to 11 in molecule **A**, and 21 to 31 in molecule **B**. Backbone and side-chain torsion angles are reported in Tables 5 and S2 (Supporting Information), respectively. Intramolecular H-bond parameters are listed in Table 6.

The conformation of the two peptide molecules is similar, as the values of corresponding backbone torsion angles in the two molecules generally do not differ by more than 4° (Table 5). Slightly larger differences, up to 10°, are observed at the level of the Gly(9)/Gly(29) and L-Ile(10)/L-Ile(30) pairs. The only other significant difference between the two molecules is the orientation of the L-Ile(10)/L-Ile(30) side chains (Table S2, Supporting Information). Not surprisingly, in view of their main-chain conformational similarity, molecules **A** and **B** adopt an identical intramolecular H-bonding scheme (Table 6).

Residue/atom numbering in the description below refers to molecule **A**. From the N-terminus, molecule **A** is characterized by the occurrence of two, consecutive *β*-turns (Venkatachalam 1968), stabilized by intramolecular H-bonds between the NH group of L-Leu(3) and the *n*Oct carbonyl oxygen, and between the NH group of L-Leu(4) and the Aib(1) carbonyl oxygen. The first *β*-turn, encompassing Aib(1) and Gly(2) as the corner residues, is of type II'. The occurrence of Aib at the $i + 1$ position of either type II or type II' *β*-turn is a rather uncommon observation (Karle and Balaram 1990; Toniolo et al. 2001b; Aravinda et al. 2008). The second *β*-turn, at the level of the

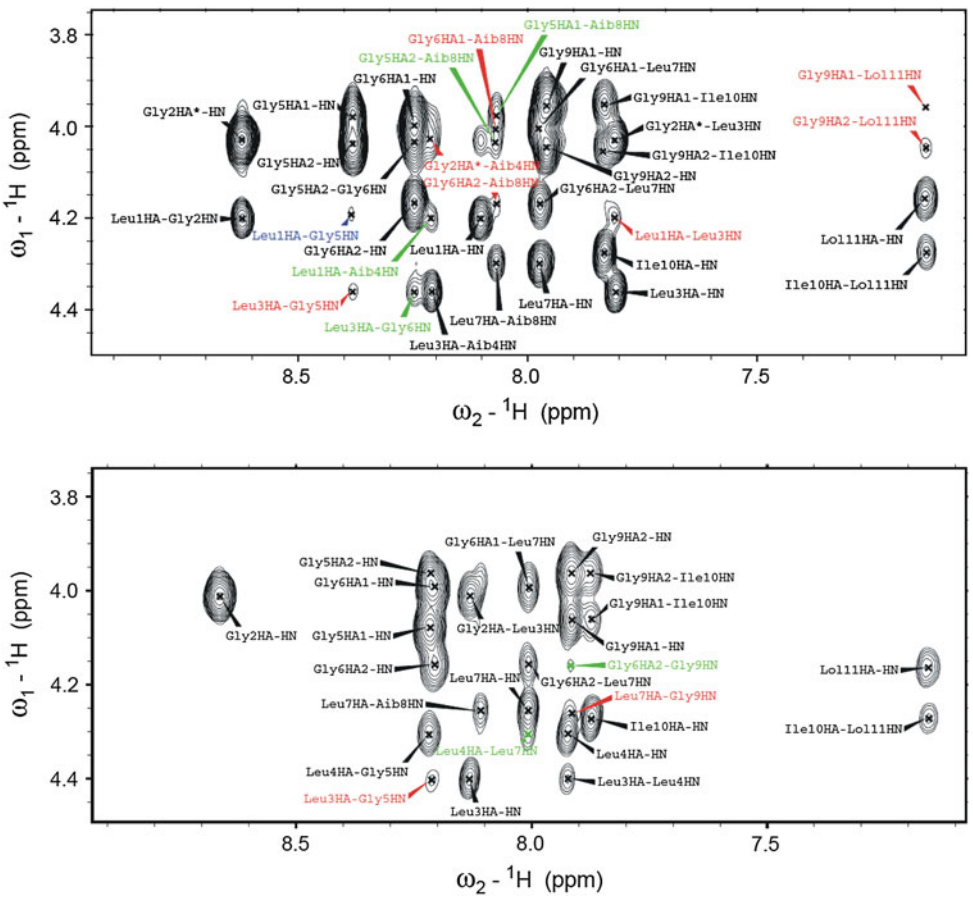

Fig. 5 Fingerprint region of the NOESY spectra of **L1** (*top*) and **L4** (*bottom*) in SDS aqueous solution (peptide concentration 1.94 and 2.74 mM, respectively). In *green*: medium-range $C^{\alpha}H_i \rightarrow NH_{i+3}$ interactions, diagnostic of the presence of an helical structure; in *red*: 3_{10}-helix $C^{\alpha}H_i \rightarrow NH_{i+2}$ cross-peaks; in *blue*: α-helix $C^{\alpha}H_i \rightarrow NH_{i+4}$ cross-peaks

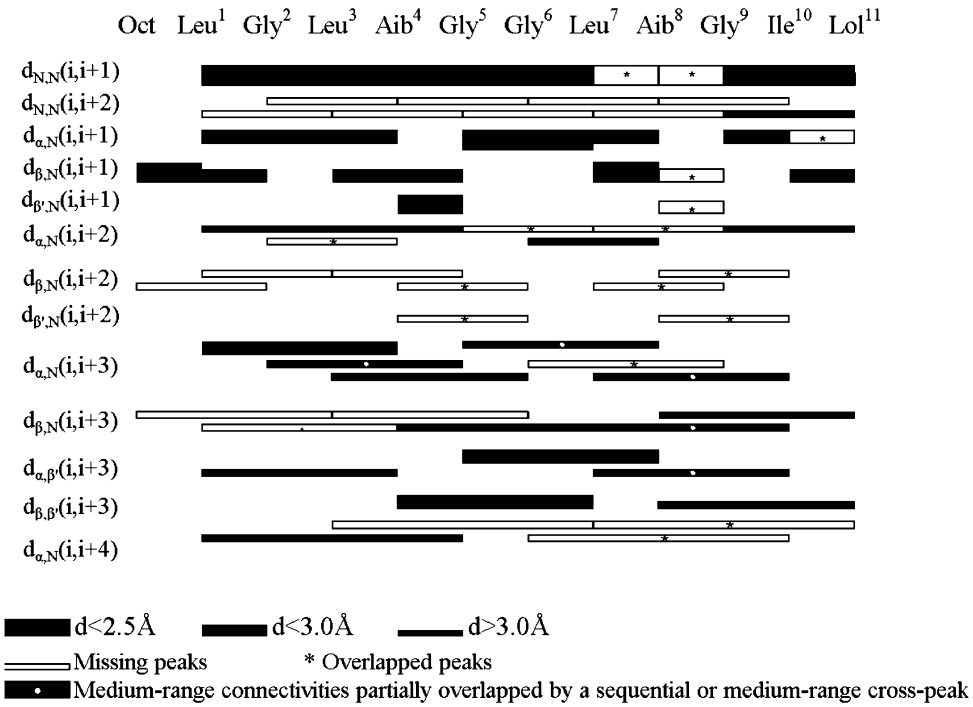

Fig. 6 Summary of the significant interresidue NOESY cross peaks for **L1** in water (9:1 H_2O/D_2O) containing (100 mM) SDS-d_{25}. Peptide concentration 1.94 mM

Gly(2)-L-Leu(3) sequence, is of type III. The set of values for the ϕ, ψ torsion angles adopted by L-Leu(4), although at the borderline of the right-handed helical region of the conformational map, does not allow for the occurrence of a direct N5–H … O2=C2 intramolecular H-bond [the N5 … O2 separation is 3.739(15) Å] that would stabilize an

Table 3 NOE constraints, deviations from idealized geometry, and mean energies for the NMR-based structures of **L1** in water (9:1 H_2O/D_2O) containing (100 mM) SDS-d_{25}

Number of NOEs	
Total	91
Intraresidue	32
Sequential	30
$i, i + n, n = 2, 3, 4$	29
Mean RMSD[a] from ideality of accepted structures	
Bonds (Å)	0.01
Angles (degree)	1.28
NOEs (Å)	0.17
Mean energies (kcal/mol) of accepted structures	
$E_{overall}$	267.5
E_{bond}	20.50
E_{angle}	71.11
E_{NOE}	44.52

[a] Root-mean-square deviation

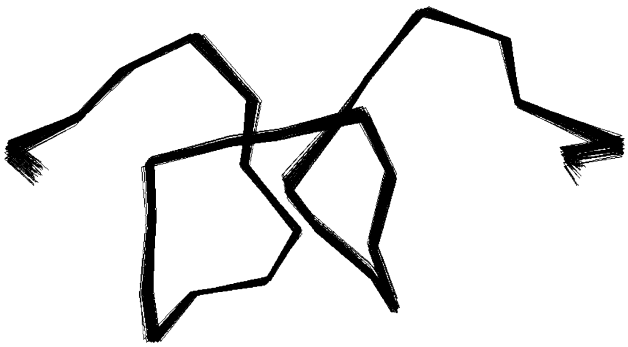

Fig. 7 Representation of the 58 3D-structures with energy <268 kcal/mol resulting from the MD calculations of **L1** with the backbone atoms superimposed

Table 4 Average values (degrees) for the torsion angles ϕ_m and ψ_m and their relative standard deviations resulting from the 59 calculated structures (energy <268.5 kcal/mol) of **L1** in water (9:1 H_2O/D_2O) containing (100 mM) SDS-d_{25}

Residue	ϕ_m	$\Delta\phi$	ψ_m	$\Delta\psi$
L-Leu[1]	−74.3	±1.4	−43.0	±0.8
Gly[2]	−67.9	±1.5	−19.1	±1.6
L-Leu[3]	−88.9	±2.3	−42.9	±0.4
Aib[4]	−73.7	±1.0	−21.9	±0.8
Gly[5]	−95.9	±1.9	−36.8	±0.8
Gly[6]	−53.5	±0.3	−42.6	±1.1
L-Leu[7]	−46.4	±0.4	−27.9	±0.3
Aib[8]	−78.4	±1.6	−38.6	±1.1
Gly[9]	−92.0	±2.0	−18.5	±0.8
L-Ile[10]	−54.3	±1.3	−27.5	±0.6
L-Lol[11]	−127.7	±3.2		

Fig. 8 Ribbon representation of the lowest energy (266.5 kcal/mol) 3D-structure obtained for **L1**. All (aliphatic) amino acid side chains are shown. The *n*Oct blocking group at position 1 was removed for clarity

additional, consecutive β-turn. Conversely, the N5-H group is H-bonded to the co-crystallized O1W water molecule which, in turn, acts as the H-bond donor to the Gly(2) carbonyl oxygen. As a result, the water molecule acts as a bridge between the N5 and O2 atoms (water-mediated, H-bonded β-turn) (Yang et al. 1979). Then, the two following Gly(5) and Gly(6) residues adopt a *quasi*-extended conformation with positive values for the ϕ torsion angle [ϕ_5, $\psi_5 = 78.7(14)°$, $177.0(11)°$; ϕ_6, $\psi_6 = 60.0(15)°$, $-166.9(9)°$]. At the level of L-Leu(7), the backbone goes back to a right-handed helical disposition that is retained, more or less irregularly, up to L-Ile(10). As a result, a non-helical C_{13} form (α-turn) (Toniolo 1980; Ramakrishnan and Nataraj 1998; Pavone et al. 1996; Chou 2000), stabilized by an intramolecular H-bond between the NH group of Gly(9) and the carbonyl oxygen of Gly(5), is followed by a short α-helical stretch in which the NH groups of L-Ile(10) and L-Lol(11) are the H-bond donors and the carbonyl oxygens of Gly(6) and L-Leu(7) are the acceptors, respectively. The helix terminates with an oxy-analog of a C_{10} form (Toniolo et al. 1986; Crisma et al. 2001), the H-bond donor of which is one of the half-occupied positions of the hydroxyl group of the C-terminal L-Lol, and the Gly(9) carbonyl oxygen is the acceptor. The NH groups of residues 1, 2, 6, 7, and 8, and the carbonyl oxygens of residues 3, 4, 8, and 10 do not take part in any direct or water-mediated intramolecular H-bonding.

The overall shape of the molecular backbone is reminiscent of a "U" letter (oriented upside down in Fig. 9), with the Gly(5)–Gly(6) segment providing connection between the two vertical arms. The orientation of the vertical arms can be approximated by two lines, one connecting the C^α atoms of Aib(1) and L-Leu(4), and the other from the L-Leu(7) to the L-Lol(11) C^α atoms. The angle between these lines is 12.2(2)° [in molecule **B** the corresponding lines make an angle of 11.4(2)°]. Most of the hydrophobic side chains and the *n*Oct aliphatic chain protrude horizontally out of the vertical arms of the "U". Conversely, all of the potential H-bonding donors and

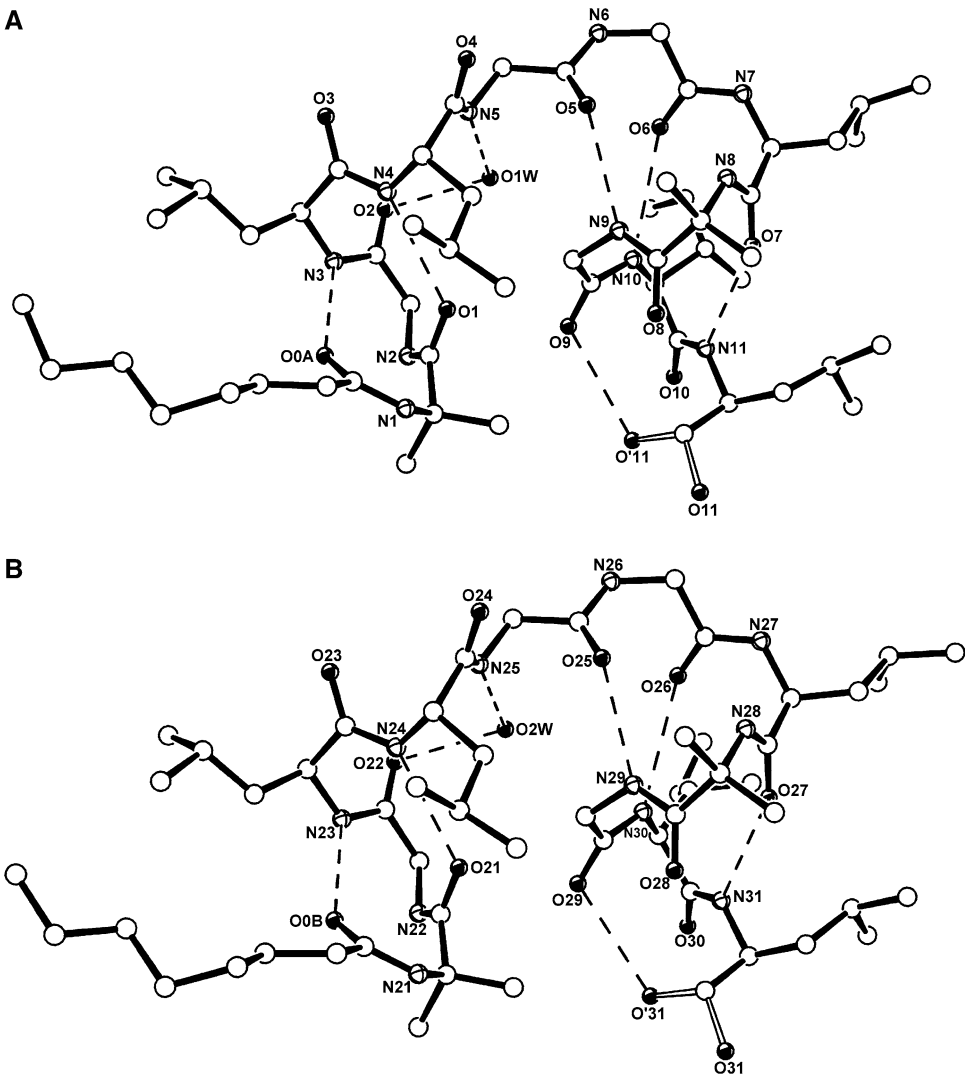

Fig. 9 X-ray diffraction structure of **L4** with heteroatom numbering. The two independent peptide molecules are indicated with **A** and **B**, respectively. Both positions of the disordered C-terminal hydroxyl groups are shown (atoms O11 and O′11 for molecule **A**, while O31 and O′31 for molecule **B**). O1W and O2W denote the two co-crystallized water molecules. Intramolecular and water-mediated hydrogen bonds are indicated by *dashed lines*

acceptors not intramolecularly engaged are located either in proximity of the Gly(5)–Gly(6) segment (atoms O3, O4, N6, N7, and N8), or close to the open edge of the two vertical arms (atoms N1, N2, O8, and O10).

It is worth recalling that the two, conformationally similar, independent peptide molecules in the X-ray diffraction structure of natural trichogin GA IV (Toniolo et al. 1994) are characterized at the N-terminus by an irregular 3_{10}-helix which evolves into a wider α-helix without any significant kink between the two helix axes. Similar, mixed 3_{10}-/α-helical conformations, spanning essentially the entire sequence, characterize also the structures of three analogs of trichogin GA IV which have been so far characterized by X-ray diffraction (Crisma et al. 1997; Monaco et al. 1999; Saviano et al. 2004). Conversely, the backbone conformation and the H-bonding pattern of **L4**, described above, quite closely mirror those of the natural compound in the 3_{10}-helical 2–4 segment and in the α-helical 7–11 segment, but are strikingly different at the level of the Gly(5)–Gly(6) sequence. It appears that in the natural sequence the Gly–Gly segment would be frozen in the helical conformation by the preceding Aib residue, but it could regain its inherent flexibility upon Aib to L-Leu replacement. Strong support to this view comes from: (1) The 3D-structure of the protected 3–7 pentapeptide segment of trichogin GA IV, Z-L-Leu-Aib-Gly–Gly-L-Leu-OMe (Crisma et al. 1996), which provides an example of retention of the helical character of the Gly–Gly sequence if preceded by an Aib residue. (2) The only other published example of an -L-Leu-Gly–Gly-L-Leu- sequence crystallographically characterized in a peptide, namely a helix-linker-β-hairpin 17-mer in which the Gly–Gly segment permits termination of the preceding helix (as a Schellman motif) (Schellman 1980) and extension to the strand segment of the C-terminal β-hairpin (Karle et al. 2000). Specifically, the first Gly is left-handed helical, while the second adopts an extended conformation characterized by positive signs of the ϕ, ψ backbone torsion angles.

Table 5 Backbone torsion angles (degree) for the X-ray diffraction structure of **L4**

Residue[a]	Molecule **A**			Molecule **B**		
	ϕ	ψ	ω	ϕ	ψ	ω
Aib(1)	44.6 (13)	−128.5 (10)	−171.9 (9)	42.1 (13)	−129.3 (10)	−171.5 (9)
Gly(2)	−65.4 (13)	−17.9 (14)	174.9 (9)	−61.7 (14)	−21.3 (14)	175.5 (9)
L-Leu(3)	−62.2 (12)	−28.0 (12)	−170.9 (9)	−62.0 (13)	−26.2 (14)	−170.0 (9)
L-Leu(4)	−65.9 (13)	−28.5 (14)	−173.5 (9)	−69.8 (13)	−29.0 (13)	−173.8 (9)
Gly(5)	78.7 (14)	177.0 (11)	−179.8 (11)	77.0 (13)	178.7 (10)	−179.7 (10)
Gly(6)	60.0 (15)	−166.9 (9)	171.2 (9)	61.5 (15)	−166.3 (10)	168.4 (10)
L-Leu(7)	−69.4 (12)	−24.3 (13)	175.6 (8)	−68.5 (14)	−28.7 (14)	178.8 (9)
Aib(8)	−50.6 (13)	−46.9 (12)	−174.1 (9)	−48.1 (13)	−49.6 (12)	−172.6 (9)
Gly(9)	−89.4 (12)	−26.2 (14)	172.9 (10)	−87.0 (12)	−31.8 (14)	179.7 (10)
L-Ile(10)	−62.0 (14)	−37.3 (15)	175.5 (11)	−67.5 (13)	−27.5 (17)	170.1 (12)
L-Lol	−92.1 (16)[b]	−177.3 (13)[c]/59.2 (16)[d]	–	−91.1 (16)[b]	−175.4 (13)[c]/59.6 (14)[d]	–

[a] Residue numbering refers to molecule **A**. For molecule **B**, add 20

[b] C10-N11-CA11-C11 in molecule **A** and C30-N31-CA31-C31 in molecule **B**, where C11/C31 refer to the L-Lol methylene carbon atom

[c] N11-CA11-C11-O11 in molecule **A** and N31-CA31-C31-O31 in molecule **B**, where O11/O31 refer to the first, half-occupied site of the hydroxyl oxygen

[d] N11-CA11-C11-O'11 in molecule **A** and N31-CA31-C31-O'31 in molecule **B**, where O'11/O'31 refer to the second, half-occupied site of the hydroxyl oxygen

Table 6 Intramolecular H-bond parameters for the X-ray diffraction structure of **L4**

D–H…A	d(D–H) (Å)	d(H…A) (Å)	d(D…A) (Å)	<DHA (°)	Symmetry equiv. of A
Intramolecular and water-mediated (molecule **A**)					
N3–H3…O0A	0.86	2.31	3.031 (12)	141	*x*, *y*, *z*
N4–H4…O1	0.86	2.23	3.065 (11)	165	*x*, *y*, *z*
N5–H5…O1W	0.86	2.27	2.89 (2)	129	*x*, *y*, *z*
O1W–H1WA…O2	0.79	1.81	2.600 (18)	178	*x*, *y*, *z*
N9–H9…O5	0.86	2.22	2.978 (13)	146	*x*, *y*, *z*
N10–H10…O6	0.86	2.44	3.247 (12)	157	*x*, *y*, *z*
N11–H11…O7	0.86	2.32	3.148 (13)	163	*x*, *y*, *z*
O′11–H'O11…O9	0.82	2.31	3.09 (3)	159	*x*, *y*, *z*
Intramolecular and water-mediated (molecule **B**)					
N23–H23…O0B	0.86	2.33	3.040 (13)	140	*x*, *y*, *z*
N24–H24…O21	0.86	2.21	3.054 (11)	167	*x*, *y*, *z*
N25–H25…O2W	0.86	2.29	2.89 (2)	127	*x*, *y*, *z*
O2W–H2WA…O22	0.84	1.81	2.649 (19)	179	*x*, *y*, *z*
N29–H29…O25	0.86	2.12	2.895 (12)	150	*x*, *y*, *z*
N30–H30…O26	0.86	2.45	3.268 (14)	160	*x*, *y*, *z*
N31–H31…O27	0.86	2.34	3.176 (13)	164	*x*, *y*, *z*
O′31–H'O31…O29	0.82	2.33	3.08 (2)	151	*x*, *y*, *z*

A comparison is also relevant with the 3D-structure of the trichodecenin I analog Z-Gly-Gly-D-Leu-Aib-Gly-D-Ile-D-Leu-OMe (Monaco et al. 1996), in that the sequence of this lipopeptaibol, (*Z*)-4-decenoyl-Gly-Gly-Leu-Aib-Gly-Ile-Lol (Fujita et al. 1994), corresponds to the 5–11 C-terminal segment of trichogin. This analog is characterized by a combination of β-turns of different handedness, which results in a non-helical, U-shaped peptide backbone. This finding suggests that deletion of the first four residues, including Aib(4), from the trichogin sequence leads to the loss of the helical character of its C-terminal segment. Finally, it is worth noting that the mixed 3_{10}-/α-helix of natural trichogin GA IV has a peculiar amphiphilic character. Indeed, all of the hydrophobic groups (the *n*Oct, L-Leu, L-Ile and L-Lol aliphatic side chains) are positioned on one helical face, and the four Gly residues comprise the

hydrophilic face. In contrast, in the case of the U-shaped **L4**, as described above, most of the hydrophobic side chains and the *n*Oct aliphatic chain protrude equatorially out of the axial arms of the "U" shape, while all of the potential H-bonding donors and acceptors not intramolecularly engaged are located either in proximity of the Gly(5)-Gly(6) segment or close to the open edge of the two axial arms. The polar groups are arranged in a way suitable to impart a hydrophilic character not only along the extremities of the open edges and the turn segment in the plane of the "U" shape, but also perpendicularly, above and below its plane. Such hydrophobic/hydrophilic pattern of the crystalline molecule seems hardly compatible with any mode of its insertion as a monomer in a lipid bilayer.

To summarize, by means of 2D-NMR and X-ray diffraction studies we found that **L1** and **L4** exhibit different conformational behaviors, namely a straight helix and a helix-loop-helix structure, respectively. In **L4**, the absence of the helix-stabilizing Aib residue in the core of the primary structure and next to the -Gly^5-Gly^6- motif, known to be inherently flexible, is probably the main responsible for the conformational behavior of this analog. Conversely, the same substitution (Aib to L-Leu) introduced at the terminal position 1 influences the helical structure only to a minor extent. Moreover, the insertion of a chiral residue (L-Leu) at this position, replacing the achiral Aib, will possibly generate a unambiguous right-handed screw-sense from the very beginning of the sequence. The distribution of the hydrophilic/hydrophobic side-chain groups within the "U-shaped" structure of **L4** seems to preclude any self-association among the peptide monomers compatible with their efficient interaction with the lipid membrane. Conversely, the structure of **L1** resembles that of the native trichogin GA IV, which is known to be prone to self-association and to interact with the lipid bilayer efficiently. Thus, we conclude that the marked difference between the conformations of **L1** and **L4** highlighted here is likely to explain their different membrane permeabilization abilities and biological properties.

Conclusions

The aim of the present work was to enhance the clear, albeit modest, amphiphilic character of the lipopeptide antibiotic trichogin GA IV by acting on the hydrophobic face of its 3D-structure. To this end, we developed a novel set of trichogin GA IV analogs, where the three Aib residues at positions 1, 4, and 8 are replaced by one or two, more hydrophobic, L-Leu residues. Leu is a known helix-supporting residue, although less effective than the non-coded Aib. The analogs were prepared by SPPS in very good yields and high levels of purity, and fully characterized. Both plasma and proteolytic stability assays underscored the remarkably long half-lives of all peptides synthesized. Our biological studies highlighted the key role played by Aib^4 on the antibacterial activity of trichogin GA IV. Indeed, the Aib to L-Leu replacement in that position (**L4** analog) makes the peptide completely inactive, while the same substitution at position 1 or 8 (**L1** and **L8** analogs) improved significantly the activity against *S. aureus*. From the results obtained from our membrane leakage assays, it turns out that the membrane permeabilization abilities of these analogs nicely parallel their antibiotic activities. We also hypothesized that the trichogin GA IV analogs described herein maintain the native membrane-targeting antibacterial mechanism. By means of 2D-NMR and X-ray diffraction studies we found that **L1** and **L4** exhibit different conformational behaviors. In particular, our X-ray diffraction study definitely demonstrated the occurrence for **L4** of a helix-loop-helix structure, which we believe likely to be largely present in solution as well. This observation might imply the occurrence of a conformational flexibility at the level of the -Gly^5-Gly^6- dipeptide sequence, enhanced by the lack of any Aib residue in its proximity. The MD calculations further indicated the presence of a clearly amphiphilic, straight helical structure for **L1** in SDS micelles. Taking into account the less effective permeabilization propensity of **L4** as compared to that of **L1** (shown by our membrane leakage assays), we suggest that their different conformations might well explain their different membrane affinities, which are probably one of the main reasons for their diverging bioactivities. **L1** and **L8**, for their significant activity against *S. aureus*, proteolytic stability, and low toxicity, represent promising leads for the development of new, peptide-based, antibacterial drugs.

Acknowledgments The authors are grateful to Prof. A. Dolmella (Department of Pharmaceutical Sciences, University of Padova) for granting access to the Gemini diffractometer and his help with X-ray diffraction data collection and processing. Financial support for the acquisition of the Agilent Technologies Gemini diffractometer was provided by the University of Padova through the 2008 "Scientific Equipment for Research" initiative.

References

Aravinda S, Shamala N, Balaram P (2008) Aib residues in peptaibiotics and synthetic sequences: analysis of nonhelical conformations. Chem Biodivers 5:1238–1262

Barlos K, Chatzi O, Gatos D, Stavropoulos G (1991) 2-Chlorotrityl chloride resin: studies on anchoring of Fmoc-amino acids and peptide cleavage. Int J Pept Protein Res 37:513–520

Bauer C, Freeman R, Frenkiel T, Keeler J, Shak AJ (1984) Gaussian pulses. J Magn Reson 58:442–457

Bax A, Davis DG (1985) MLEV-17-based two-dimensional homonuclear magnetization transfer spectroscopy. J Magn Reson 65:355–360

Bax A, Subramanian S (1986) Sensitivity-enhanced two-dimensional heteronuclear shift correlation NMR spectroscopy. J Magn Reson 67:565–569

Bax A, Summers MF (1986) Proton and carbon-13 assignments from sensitivity-enhanced detection of heteronuclear multiple-bond connectivity by 2D multiple quantum NMR. J Am Chem Soc 108:2093–2094

Bax A, Griffey RH, Hawkins BL (1983) Correlation of proton and nitrogen-15 chemical shifts by multiple quantum NMR. J Magn Reson 55:301–315

Bellamy LJ (1966) The infrared spectra of complex molecules, 2nd edn. Methuen, London

Benedetti E, Di Blasio B, Pavone V, Pedone C, Toniolo C, Crisma M (1992) Characterization at atomic resolution of peptide helical structures. Biopolymers 32:453–456

Beychock S (1967) Circular dichroism of poly-α-amino acids and proteins. In: Fasman GD (ed) Poly-α-amino acids: protein models for conformational studies. Dekker, New York, pp 293–337

Bollhagen R, Schmiedberger M, Barlos K, Grell E (1994) A new reagent for the cleavage of fully protected peptides synthesised on 2-chlorotrityl chloride resin. J Chem Soc Chem Commun 22:2559–2560

Brogden KA (2005) Antimicrobial peptides: pore formers or metabolic inhibitors in bacteria? Nat Rev Microbiol 3:238–250

Brückner H, Maisch J, Reinecke C, Kimonyo A (1991) Use of α-aminoisobutyric acid and isovaline as marker amino acids for the detection of fungal polypeptide antibiotics. Screening of Hypocrea. Amino Acids 1:251–257

Chou KC (2000) Prediction of tight turns and their types in proteins. Anal Biochem 286:1–16

Chugh JK, Wallace BA (2001) Peptaibols: models for ion channels. Biochem Soc Trans 29:565–570

Crisma M, Valle G, Monaco V, Formaggio F, Toniolo C (1996) Molecular and crystal structures of terminally protected tri- and pentapeptides of trichogin GA IV. Zeit Crystallogr 211:528–532

Crisma M, Monaco V, Formaggio F, Toniolo C, George C, Flippen-Anderson JL (1997) Crystallographic structure of a helical lipopeptaibol antibiotic analogue. Lett Pept Sci 4:213–218

Crisma M, Barazza A, Formaggio F, Kaptein B, Broxterman QB, Kamphuis J, Toniolo C (2001) Peptaibolin: synthesis, 3D-structure, and membrane modifying properties of the natural antibiotic and selected analogues. Tetrahedron 57:2813–2825

Cung MT, Marraud M, Néel J (1972) Étude expérimentale de la conformation de molécule dipeptidiques. Comparison avec les prévision théoriques. Ann Chim (Paris) 183–209

De Zotti M, Biondi B, Formaggio F, Toniolo C, Stella L, Park Y, Hahm K-S (2009) Trichogin GA IV: an antibacterial and protease-resistant peptide. J Pept Sci 15:615–619

De Zotti M, Biondi B, Peggion C, Park Y, Hahm K-S, Formaggio F, Toniolo C (2011) Synthesis, preferred conformation, protease stability, and membrane activity of heptaibin, a medium-length peptaibiotic. J Pept Sci 17:585–594

De Zotti M, Biondi B, Peggion C, Formaggio F, Park Y, Hahm K-S, Toniolo C (2012) Trichogin GA IV: a versatile template for the synthesis of novel peptaibiotics. Org Biomol Chem 10:1285–1299

Degenkolb T, Berg A, Gams W, Schlegel B, Gräfe U (2003) The occurrence of peptaibols and structurally related peptaibiotics in fungi and their mass spectrometric identification via diagnostic fragment ions. J Pept Sci 9:666–678

Emsley L, Bodenhausen G (1989) Self-refocusing effect of 27° Gaussian pulses. Applications to selective two-dimensional exchange spectroscopy. J Magn Reson 82:211–221

Formaggio F, Crisma M, Rossi P, Scrimin P, Kaptein B, Broxterman QB, Kamphuis J, Toniolo C (2000) The first water-soluble 3_{10}-helical peptides. Chem Eur J 6:4498–4504

Formaggio F, Broxterman QB, Toniolo C (2003) In: Goodman M, Felix A, Moroder L, Toniolo C (eds) Houben-Weyl: methods of organic chemistry. Synthesis of peptides and peptidomimetics, vol E22c. Thieme, Stuttgart, pp 292–310

Fujita T, Wada S, Iida A, Nishimura T, Kanai M, Toyama N (1994) Fungal metabolites. xiii. Isolation and structural elucidation of new peptaibols, trichodecenins-I and -II, from *Trichoderma viride*. Chem Pharm Bull 42:489–494

Gordon Y, Huang L, Romanowski E, Yates K, Proske R, McDermott A (2005) Human cathelicidin (LL-37), a multifunctional peptide, is expressed by ocular surface epithelia and has potent antibacterial and antiviral activity. Curr Eye Res 30:385–394

Griesinger C, Otting G, Wüthrich K, Ernst RR (1988) Clean TOCSY for proton spin system identification in macromolecules. J Am Chem Soc 110:7870–7872

Hancock REW, Sahl H-G (2006) Antimicrobial and host-defense peptides as new anti-infective therapeutic strategies. Nat Biotechnol 24:1551–1557

Hjørringgaard CU, Pedersen JM, Vosegaard T, Nielsen NC, Skrydstrup T (2009) An automatic solid-phase synthesis of peptaibols. J Org Chem 74:1329–1332

Karle IL, Balaram P (1990) Structural characteristics of α-helical peptide molecules containing Aib residues. Biochemistry 29:6747–6756

Karle IL, Das C, Balaram P (2000) De novo protein design: crystallographic characterization of a synthetic peptide containing independent helical and hairpin domains. Proc Natl Acad Sci USA 97:3034–3037

Kocsis L, Ruff F, Orosz G (2006) The effect of peptide length on the cleavage kinetics of 2-chlorotrityl resin-bound ethers. J Pept Sci 12:428–436

Korady R, Billeter M, Wüthrich K (1996) MOLMOL: a program for display and analysis of macromolecular structures. J Mol Graph 14:51–55

Manning MC, Woody RW (1991) Theoretical CD studies of polypeptide helices: examination of important electronic and geometric factors. Biopolymers 31:569–586

Marr AK, Gooderham WJ, Hancock REW (2006) Antibacterial peptides for therapeutic use: obstacles and realistic outlook. Curr Opin Pharmacol 6:468–472

Mazzuca C, Stella L, Venanzi M, Formaggio F, Toniolo C, Pispisa B (2005) Mechanism of membrane activity of the antibiotic trichogin GA IV: a two-state transition controlled by peptide concentration. Biophys J 88:3411–3421

Monaco V, Formaggio F, Crisma M, Toniolo C, Shui X, Eggleston DS (1996) Crystallographic structure of a multiple β-turn containing, glycine-rich heptapeptide: a synthetic precursor of the lipopeptaibol antibiotic trichodecenin I. Biopolymers 39:31–42

Monaco V, Locardi E, Formaggio F, Crisma M, Mammi S, Peggion E, Toniolo C, Rebuffat S, Bodo B (1998) Solution conformational analysis of amphiphilic helical, synthetic analogs of the lipopeptaibol trichogin GA IV. J Pept Res 52:261–272

Monaco V, Formaggio F, Crisma M, Toniolo C, Hanson P, Millhauser G, George C, Deschamps JR, Flippen-Anderson JL (1999) Determining the occurrence of a 3_{10}-helix and an α-helix in two different segments of a lipopeptaibol antibiotic using TOAC, a nitroxide spin-labeled C^{α}-tetrasubstituted α-aminoacid. Bioorg Med Chem 7:119–131

Moretto V, Crisma M, Bonora GM, Toniolo C, Balaram H, Balaram P (1989) Comparison of the effect of five guest residues on the β-sheet conformation of host (L-Val)*n* oligopeptides. Macromolecules 22:2939–2944

Papo N, Shai Y (2005) Host defense peptides as new weapons in cancer treatment. Cell Mol Life Sci 62:784–790

Pavone V, Gaeta G, Lombardi A, Nastri F, Maglio O, Isernia C, Saviano M (1996) Discovering protein secondary structures: Classification and description of isolated α-turns. Biopolymers 38:705–721

Peggion C, Formaggio F, Crisma M, Epand RF, Epand RM, Toniolo C (2003) Trichogin: a paradigm for lipopeptaibols. J Pept Sci 9:679–689

Pysh ES, Toniolo C (1977) Conformational analysis of protected norvaline oligopeptides by high resolution proton nuclear magnetic resonance. J Am Chem Soc 99:6211–6219

Ramakrishnan C, Nataraj DV (1998) Energy minimization studies on α-turns. J Pept Sci 4:239–252

Rance M, Sørensen OW, Bodenhausen G, Wagner G, Ernst RR, Wüthrich K (1983) Improved spectral resolution in COSY ^{1}H NMR spectra of proteins via double quantum filtering. Biochem Biophys Res Commun 117:479–485

Saviano M, Improta R, Benedetti E, Carrozzini B, Cascarano GL, Didierjean C, Toniolo C, Crisma M (2004) Benzophenone photophore flexibility and proximity: molecular and crystal-state structure of a Bpa-containing trichogin dodecapeptide analogue. ChemBioChem 5:541–544

Schellman C (1980) In: Jaenicke R (ed) Protein folding. Elsevier, Amsterdam, pp 53–61

Schwieters CD, Kuszewski JJ, Tjandra N, Clore GM (2003) The Xplor-NIH NMR molecular structure determination package. J Magn Reson 160:65–74

Sheldrick GM (2008) A short history of SHELX. Acta Crystallogr 64A:112–122

Smeazzetto S, De Zotti M, Moncelli MR (2011) A new approach to detect and study ion channel formation in microBLMs. Electrochem Commun 13:834–836

Toniolo C (1980) Intramolecularly hydrogen-bonded peptide conformations. CRC Crit Rev Biochem 9:1–44

Toniolo C, Benedetti E (1991) The polypeptide 3_{10}-helix. Trends Biochem Sci 16:350–353

Toniolo C, Brückner H (2009) Peptaibiotics: fungal peptides containing α-dialkyl α-amino acids. Wiley-VCD, Weinheim/Zürich

Toniolo C, Valle G, Bonora GM, Crisma M, Formaggio F, Bavoso A, Benedetti E, Di Blasio B, Pavone V, Pedone C (1986) A novel peptide conformation: first unequivocal observation of the oxy-analog of a β-bend. Biopolymers 25:2237–2253

Toniolo C, Peggion C, Crisma M, Formaggio F, Shui X, Eggleston DS (1994) Structure determination of racemic trichogin A IV using centrosymmetric crystals. Nat Struct Biol 1:908–914

Toniolo C, Crisma M, Formaggio F, Peggion C, Monaco V, Goulard C, Rebuffat S, Bodo B (1996a) Effect of N^{α}-acyl chain length on the membrane-modifying properties of synthetic analogs of the lipopeptaibol trichogin GA IV. J Am Chem Soc 118:4952–4958

Toniolo C, Polese A, Formaggio F, Crisma M, Kamphuis J (1996b) Circular dichroism spectrum of a peptide 3_{10}-helix. J Am Chem Soc 118:2744–2745

Toniolo C, Crisma M, Formaggio F, Peggion C, Epand RF, Epand RM (2001a) Lipopeptaibols, a novel family of membrane active, antimicrobial peptides. Cell Mol Life Sci 58:1179–1188

Toniolo C, Crisma M, Formaggio F, Peggion C (2001b) Control of peptide conformation by the Thorpe-Ingold effect (C^{α}-tetrasubstitution). Biopolymers (Pept Sci) 60:396–419

Tossi A, Sandri L, Giangaspero A (2000) Amphipathic, α-helical antimicrobial peptides. Biopolymers (Pept Sci) 55:4–30

Venkatachalam CM (1968) Stereochemical criteria for polypeptides and proteins. V. Conformation of a system of three linked peptide units. Biopolymers 6:1425–1436

Weigelt S, Huber T, Hofmann F, Jost M, Ritzefeld M, Luy B, Freudenberger C, Majer Z, Vass E, Greie J-C, Panella L, Kaptein B, Broxterman QB, Kessler H, Altendorf M, Hollósi M, Sewald N (2012) Synthesis and conformational analysis of efrapeptins. Chem Eur J 18:478–487

Wüthrich K (1986) NMR of proteins and nucleic acids. Wiley, New York

Yamaguchi H, Kodama H, Osada S, Kato F, Jelokhani-Niaraki M, Kondo M (2003) Effect of α,α-dialkyl amino acids on the protease resistance of peptides. Biosci Biotechnol Biochem 67:2269–2272

Yang C-H, Brown JN, Kopple KD (1979) Peptide–water association in peptide crystals. Int J Pept Protein Res 14:12–20

Zasloff M (2002) Antimicrobial peptides of multicellular organisms. Nature 415:389–395

Zhang L, Falla TJ (2006) Antimicrobial peptides: therapeutic potential. Expert Opin Pharmacother 7:653–663